Chemical Engineering Journal 284 (2016) 1342–1347

Contents lists available at ScienceDirect

Chemical Engineering Journal

journal homepage: www.elsevier.com/locate/cej

Performance study of pervaporation in a microfluidic system for the removal of acetone from water

Yali Zhang [a], Nieck E. Benes [b], Rob G.H. Lammertink [a,*]

[a] Soft Matter, Fluidics and Interfaces, MESA+ Institute for Nanotechnology, Faculty of Science and Technology, University of Twente, Enschede, The Netherlands
[b] Films in Fluids/Inorganic Membranes, MESA+ Institute for Nanotechnology, Faculty of Science and Technology, University of Twente, Enschede, The Netherlands

HIGHLIGHTS

- We report an efficient μ-PV device to separate acetone from water.
- 81% acetone is removed within just 3 min at room temperature.
- Our microfluidic device provides insight in the mass transport limitations.
- A design criterion is derived to characterise and optimise the PV process.
- Promising potential as a universal tool to remove VOCs from water in microscale.

ARTICLE INFO

Article history:
Received 28 July 2015
Received in revised form 21 September 2015
Accepted 24 September 2015

Keywords:
Pervaporation
Microfluidic
Mass transfer
Modelling
VOCs

ABSTRACT

Separation of organic compounds from aqueous streams presents many challenges regarding materials and separation conditions. Such separations become increasingly important with the development of biomass related processes. Pervaporation is a promising membrane process capable of isolating organic species from aqueous feeds. Typically, volatile organic compounds (VOCs) removal from water suffers from mass transport limitations due to depletion of the minor component at the membrane surface. Understanding of such mass transport limitations is crucial for the development of novel pervaporation membranes and methods. In this work, we present a performance study on the removal of trace amount of acetone from water via pervaporation to provide insight on mass transport limitations. We used glass microfluidics containing a thin polydimethylsiloxane (PDMS) membrane that allows very fast removal of acetone from water. Via modelling and experiments, we quantitatively investigate the mass transfer coefficients of acetone through the liquid boundary layer (k_l) and that of the membrane (k_m) by varying membrane thicknesses and feed flow rates. High acetone removal efficiency of 81% is achieved for just 3 min residence time at room temperature for a 35 μm thin membrane. A design criterion based on intrinsic system parameters is derived to engineer the pervaporation system for both micro- and macro-scales. Our micro-PV device shows promising potential regarding the characterisation of pervaporation processes and materials for the removal of VOCs from water.

1. Introduction

The broad ranges of functionality and versatility of microchemical systems has promoted their transformation from simple devices, like micro-reactors [1–3], micro-mixers [4,5], and micro-separators [6,7], to complex multi-step integrated networks [8–11]. Developing a continuous multi-step microchemical synthesis is of particular interests nowadays. Moreover, such systems provides fundamental insight regarding the mass transport kinetics.

Separating immiscible liquids in microdevices has been intensively investigated exploiting capillary phenomena which become stronger at smaller length scales [12,13]. Separating miscible liquids requires different approaches. Trace removal of volatile organic compounds (VOCs) from water inherently suffers from mass transport limitations posing challenges regarding fast and complete purification. Few studies have attempted to accomplish microfluidic separation by implementing membrane technology [14,15]. Zhang et al. [14] reported membrane distillation in a microfluidic system to separate water-methanol mixtures. By

* Corresponding author.
E-mail address: r.g.h.lammertink@utwente.nl (R.G.H. Lammertink).

http://dx.doi.org/10.1016/j.cej.2015.09.084
1385-8947/

generating a temperature gradient in a stacked microdevice, methanol vapour was separated from water and collected in a cooling channel. Kaufman et al. [15] fabricated a high pressure microfluidic cell for Nanofiltration/Reverse Osmosis separation. They have investigated the performance of the device via both experiments and simulation and concluded that a shallower channel is beneficial for minimising concentration polarisation. In addition to these membrane technologies in microdevices, pervaporation (PV) seems another interesting but relatively unexplored candidate.

PV is an efficient membrane process to separate minor components from liquid mixtures by partial vapourisation and permeation. Such process is performed by bringing a liquid mixture in contact with one side of a membrane while a vacuum or a sweeping gas is applied to the other side. Species with higher affinities for the membrane, diffuse preferentially through the membrane and vapourise at the other side of the membrane. The created concentration gradient or the partial pressure difference across the membrane is the driving force for the separation process. The advantages of PV, regarding energy requirements and simple process control, allow for competitive applications like separating VOCs from water, aqueous acrylic latex, dehydrating organic solvents, and organic-organic solvent separation [16–20]. The study of VOC pervaporation using microfluidic devices is of particular interest due to the notorious concentration polarisation, or depletion, resulting in severe mass transport limitations.

Implementing pervaporation into microfluidic devices has been accomplished in some examples [21–24]. Transport of water through a polydimethylsiloxane (PDMS) layer was used to investigate concentration profiles and phase diagrams of the retained solute [22,25,26]. Ziemecka has recently reported progress on concentrating hydrogen peroxide by pervaporation in a microfluidic device by varying the process temperatures. The experimental results closely resembled their 1D modelling work. No investigation on the mass transport resistance was reported in their study [24]. Among these studies, PDMS membranes are commonly selected as a results of their properties including optical transparency, ease of integration into microdevices and low-cost.

The mass transport mechanisms of PV systems can be described in various models according to the selection of dense or porous membranes [27–30]. The resistance-in-series model is widely accredited in describing the mass transport for dense membrane pervaporation systems under steady state. Three serial mass transfer resistances are defined in this model (Eq. (1) and (2)); the resistance in the feed liquid ($1/k_l$), that across the membrane ($1/k_m$) and that in the membrane permeate ($1/k_p$). The $1/k_p$ is normally neglected due to relatively fast transport in the gas phase. The permeation flux J_m of the migrating species in the system can be defined as

$$J_m = k_{ov}(c_l - c_p) = k_l(c_l - c_{l,m}) = k_m(c_{l,m} - c_{m,p}) \quad (1)$$

where $c_l, c_p, c_{l,m}$ and $c_{m,p}$ ($mole\ m^{-3}$) are the species concentrations in the feed bulk, in the permeate phase, at the feed-membrane interface and at the membrane-permeate interface, respectively. k_{ov} ($m\ s^{-1}$) is the overall mass transfer coefficient. The inverse of a mass transfer coefficient is the respective resistance:

$$\frac{1}{k_{ov}} = \frac{1}{k_l} + \frac{1}{k_m} = \frac{l}{D} + \frac{\delta}{D_m} \quad (2)$$

where δ is the membrane thickness, D_m is the species diffusion coefficient in the membrane, D is its diffusion coefficient in the solvent, and l is the thickness of the concentration boundary layer in the liquid feed.

The values of k_m and k_l allow comparisons of process performances, as well as evaluations of mass transfer efficiency for different configurations. It is important to notice that k_l varies with the dynamics of the feed solution and k_m depends on the intrinsic membrane characteristics. Côté and Lipski [31,32] are among the first to propose that the mass transfer of a PV system is particularly limited by diffusion of the solute in the boundary layer. The reason lies in the long diffusion length or low concentration gradient between the bulk to the membrane boundary which cause strong concentration polarisation. Depletion in the boundary layer can dominate the performance [33]. In particular, Wijmans shows that concentration polarisation already dominates at very low Peclet (Pe) numbers for the removal of trace compounds by PV [34]. In such a case, membrane selection is less critical. Relative thick rubber membranes are sufficient and preferable over thinner composite materials due to the advantages in low-cost and low water permeability. Li et al. [35] have investigated operation parameters on the PV performance using a composite PDMS membrane to separate a variety of organic solvents from water. Their results have shown a high dependence of the dominant resistance region on the solvent properties, particularly in its partition coefficient. In their investigated flow rate range, methanol transfer is limited by the k_m whereas acetone transfer is determined by both k_m and k_l.

In this study, we aim to conduct a performance study for the removal of acetone from water to provide the insights on the mass transport mechanisms. The used microfluidic format provides excellent mass transport in the boundary layer, which allows adequate membrane performance assessment. A thin layer of PDMS membrane was selected for its high selectivity for VOCs in a low concentration range [36,37]. Via modelling and experiments, we quantitatively investigated the local mass transfer coefficients of acetone through the liquid boundary layer (k_l) and the membrane (k_m) by varying membrane thicknesses and feed flow rates. An optimisation based on the intrinsic system parameters is proposed to identify the rate limiting region and engineer the design for both micro- and macro-scale pervaporation.

2. Experimental

2.1. Microchips preparation

Glass slides. The microchannels for liquid flow (L-channel) and gas flow (G-channel) were fabricated on separate borofloat glass slides by standard photolithography followed by wet etching (Micronit B.V.). The depth (H) and length (L) of both channels were 50 μm and 0.26 m, respectively. The width of the L-channel was 350 μm and the G-channel was 600 μm to facilitate channel alignment during manual assembly (Fig. 1). The glass slides were diced in the size of 1.5 × 4.5 cm for bonding.

PDMS membrane. The flat-sheet PDMS membranes were prepared by mixing the polymer and the crosslinking agent (TRV 615 A+B, Momentive, Columbus, Ohio) in 10:1 weight ratio [38]. The mixture was first degassed in a desiccator and then cast onto a polished aluminium plate at controlled thickness. The films were cured at 80° for 2 h in a nitrogen-flushed oven and then placed in a nitrogen box overnight. The resulting membrane thicknesses were measured by a Micrometer (Coolant Proof) at multiple spots of the membranes before bonding and varied between 35–270 ± 5 μm.

Membrane integration. A combined oxygen plasma and thermal-bonding method was employed to create leakage-free bonding between PDMS membrane and glass slides [39]. Two glass slides and a PDMS membrane were firstly cleaned and activated by oxygen plasma at 60 W, 40 s (Femto, Diener Electronic). The PDMS membrane was immediately contacted with one glass slide first and then to the other with manual alignment. The pre-bonded chip was clamped and placed in an oven to enhance the bonding strength at 80° for 2 h. The bonded chip was enclosed in a Micronit

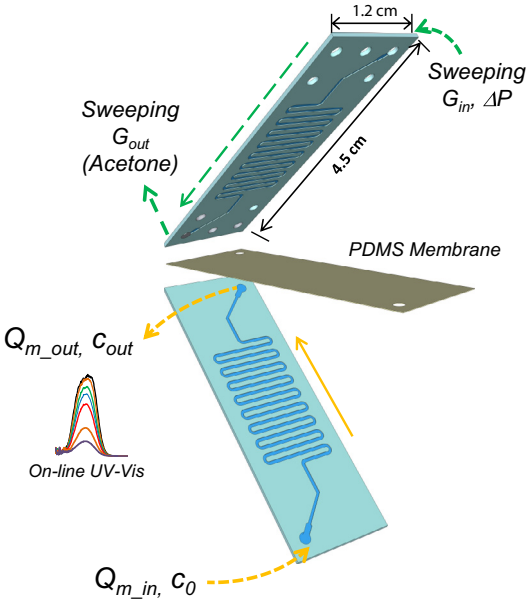

Fig. 1. Schematic illustration of the glass chip with a thin layer of PDMS membrane in between. The concentration in the outlet is analysed online using UV–Vis spectroscopy.

chip holder and connected (Upchurch connections) to the gas and liquid flow control. Both mass and concentration measurements at the in- and outlets were performed before each measurement to ensure a leakage-free operation of the microchip.

2.2. Experimental setup

The aqueous feed solutions were prepared by dissolving acetone (Sigma–Aldrich) in deionized water at 0.2 wt% and 0.4 wt% and pumped into the L-channel under flow rates (q_v) ranging from 1 to 10 μL min^{-1} using a syringe pump (HARVARD Apparatus PHD 2000). The corresponding residence times (V/q_v, V is the channel volume) and Reynolds numbers (Re) range from 26 to 264 s and 0.08 to 0.84, respectively. A co-sweeping nitrogen flow was pumped through the G-channel under a constant feed pressure of 0.120 bar (Bronkhost EL-PRESS). This pressure has been verified experimentally to ensure a gas flow independent acetone removal. The acetone concentration in the liquid outflow was detected by light absorbance measurement using an online UV-Vis spectrophotometer (Ocean optics, DH-2000). Acetone was selected as the target solute due to its unique absorption peak within the wavelength of UV–Vis range. The calibration curve was measured for concentrations from 0.01 to 0.8 wt% at the wavelength of 262.64 nm. Only feed concentrations lower than 0.4 wt% were prepared for the measurements as a result of their linear correlation to the corresponding absorbance in this range (Fig. 2). All experiments were conducted at room temperature and for multiple runs. The sensitivity of the setup provided standard deviations that were smaller than the symbols used in the plots. The normalised average outlet concentration c_{out}/c_0 was determined to evaluate the acetone removal efficiency at various τ and membrane thicknesses.

3. Modelling

A boundary flux condition describing the membrane transport, coupled with the convection-diffusion equation for the L-channel were used to investigate the mass transport evolution of acetone from the L-channel through the membrane. Fig. 3 illustrates the L-channel and the PDMS membrane with indicated transport resistances. The G-channel resistance was ignored by assuming a zero acetone concentration in the gas phase. It was reported that varying feed concentration and temperature has minor influence on the PDMS membrane selectivity between acetone and water [37]. Here, we consider only acetone migration through the PDMS membrane. The acetone flux through the membrane under steady state is proportional to the permeability P, the membrane thickness δ, and the partial vapour pressure at the membrane surface p_l (Eq. (3)). The right-hand side of the Eq. (3) gives the solute flux arriving at the membrane wall from the bulk due to diffusion. The left hand side of the equation accounts for solute flux through the PDMS membrane.

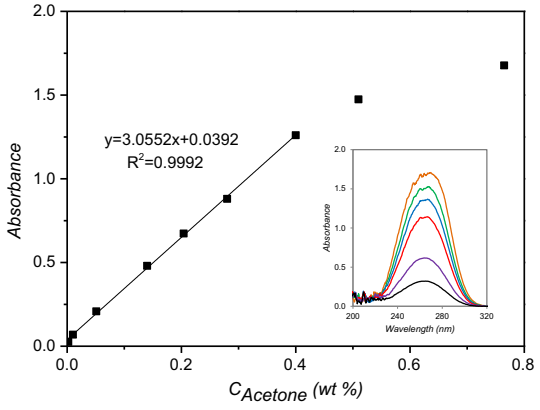

Fig. 2. Calibration curve for acetone relating the bulk concentration to its absorbance measured by UV–Vis.

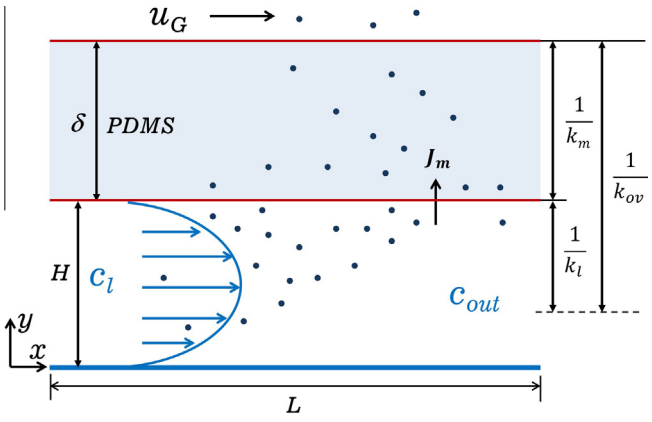

Fig. 3. Illustration of the 2D numerical model, assuming a parabolic velocity profile in the liquid phase, with purely advective transport in the x direction and only diffusion in the y direction.

$$J_m = \frac{P}{\delta} p_l = -D \left.\frac{\partial c_l}{\partial y}\right|_{y=H} \tag{3}$$

where D is the diffusion coefficient of acetone in water, and c_l the acetone concentration at the membrane. By using Henry's law, $Kp_l = c_l$, where K is the Henry constant, we obtain a simple boundary condition for the convection diffusion domain (at $y = H$):

$$\left.\frac{\partial c_l}{\partial y}\right|_{y=H} = -\frac{P}{\delta K D} c_l \tag{4}$$

The factor $P/\delta K$ can be collapsed into the membrane mass transfer coefficient k_m. By implementing the channel configuration, the non-dimensional boundary condition for $y = H$ is obtained:

$$\left.\frac{\partial \tilde{c}_l}{\partial \tilde{y}}\right|_{\tilde{y}=1} = -\frac{Hk_m}{D}\tilde{c}_l \tag{5}$$

where $\tilde{y} = y/H$ and $\tilde{c}_l = c_l/c_0$. The dimensionless parameter Hk_m/D, which is the ratio of the membrane flux to the diffusive flux and defined as our performance number, fully determines the performance of the separation and can be used to understand and optimise the process. Realise that our performance number is equivalent to the second Damköhler number typically used for surface reactions, where we use k_m as the mass transfer rate of the membrane instead of a first order surface reaction rate constant.

As the acetone concentration is lower than 1 wt%, its presence in the bulk stream will not affect the density and the velocity profile of the flow significantly [40]. The transport in the liquid phase is governed by the convection diffusion equation:

$$u(y)\frac{\partial c_l}{\partial x} = D\frac{\partial^2 c_l}{\partial y^2} \tag{6}$$

where $u(y) = u_{avg}(-6y^2/H^2 + 6y/H)$ is the parabolic velocity profile. The convection diffusion equation is non-dimensionalised by introducing $\tilde{x} = x/L$, and previously introduced $\tilde{y}$ and $\tilde{c}_l$, to result in:

$$\frac{6u_{avg}H^2}{LD}(-\tilde{y}^2 + \tilde{y})\frac{\partial \tilde{c}_l}{\partial \tilde{x}} = \frac{\partial^2 \tilde{c}_l}{\partial \tilde{y}^2} \tag{7}$$

Realize that the dimensionless factor on the left side of the Eq. (7), $u_{avg}H^2/LD$, equals the transverse Peclet number Pe_m times the ratio of height-to-length ($\alpha = H/L$) (Eq. (8)) [41]. This number represents the ratio of timescales for diffusion in the normal ($\perp$) and advection in the tangential ($\parallel$ convection) direction.

$$\alpha Pe_m = \frac{\tau_\perp}{\tau_\parallel} = \frac{u_{avg}H^2}{LD} \tag{8}$$

Together with the dimensionless parameter from the boundary condition, Hk_m/D, these numbers indicate the different regimes for transport and possible concentration polarisation significance. Steady state concentration profiles are computed by solving Eq. (7) with boundary condition (5) in Matlab for k_m values ranging from 10^{-6} to 10^{-8} m s^{-1}. The lower boundary, at $y = 0$ is considered as impermeable. The numerical results were fitted to the experimental results to extract the values of $k_{m,2D}$ for different membrane thicknesses.

4. Results and discussion

Due to the microfluidic dimensions and consequently well-defined flow conditions, the mass transport evolution of the PV system can be accurately studied. We have conducted a systematic study on the performance of the PV system by varying the feed concentration, membrane thickness and flow rate. Their influence on the separation efficiency has been investigated and represented in terms of k_m and k_l values. The comparison of k_m and k_l values indicates the dominant mass transport resistance, which allows an optimisation of the PV system.

We have first investigated the effect of feed concentration on the acetone separation efficiency. Fig. 4 reveals the evolution of c_{out}/c_0 as a function of τ for membrane thicknesses of 35 and 270 μm, respectively. As can be seen, the inlet feed concentration has minor effect on the c_{out}/c_0 under the experimental conditions used [42]. This confirms a constant membrane permeability k_m for the different feed concentrations.

To determine the k_m values, we have prepared PDMS membranes with different thicknesses from the same batch to ensure a constant permeability. Fig. 5 reveals the influence of membrane thickness on the normalised outlet concentration c_{out}/c_0 as a function of τ. The symbols represent the experimental results and lines are the fitted simulation results. Both the membrane thickness and residence time τ have pronounced influence on the acetone separation efficiency.

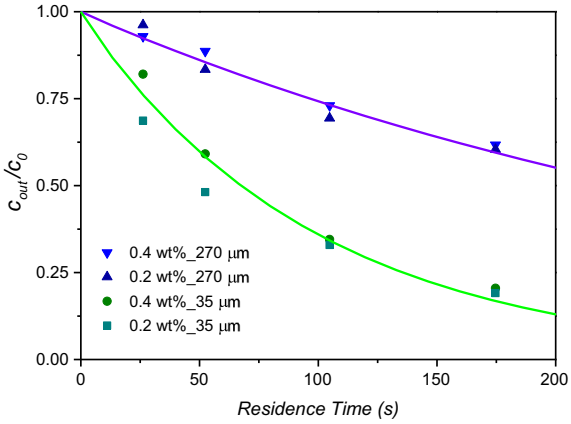

Fig. 4. c_{out}/c_0 against residence time for different feed concentrations and membrane thicknesses.

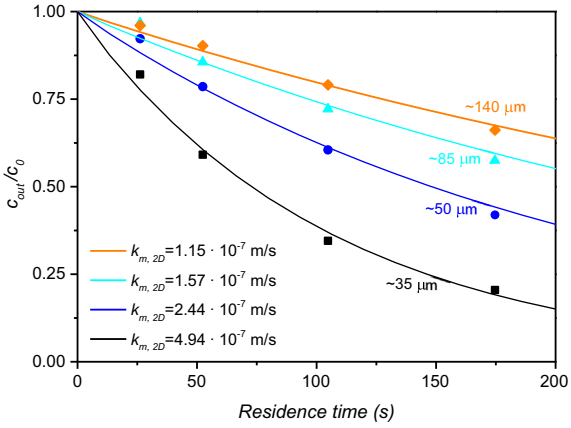

Fig. 5. c_{out}/c_0 against residence time with different membrane thicknesses. Symbols represent the experimental results and lines correspond to the fitted simulation results. $c_0 = 0.4$ wt%.

The k_m values of each membrane thickness are extracted by fitting the 2D simulation results for τ ranging from 53 to 170 s where the experimental results are most reliable. The weighted standard deviation is minimised as the optimisation function (Eq. (9)). The obtained k_m values range from 1.15 to 4.94 · 10^{-7} m s^{-1} for the indicated film thicknesses. These values are consistent with those of scaled PV systems. The extracted permeability of the PDMS membrane towards acetone is then on the order of 10^{-11} m^2 s^{-1} (comparable to 9 · 10^{-11} m^2 s^{-1} for 8 μm composite PDMS membrane [35]).

$$\sigma_w = \sqrt{\frac{\sum_{i=1}^{n}((c_{exp} - c_{sim})/c_{exp})^2}{N-1}} \tag{9}$$

Since our 2D model includes the axial convection and transverse diffusion, we fully capture any depletion zone forming. A simpler 1D model can be applied when neglecting any normal concentration gradients (in the y direction), and the concentration is only a function along the x position in the channel. Such a 1D model describes convective transport in x-direction equals to the removal rate through the membrane:

Table 1
Comparison of the k_m values in between 1D and 2D models.

Membranes (μm)	k_m 2D (m s^{-1})	k_m 1D (m s^{-1})
35	$4.94 \cdot 10^{-7}$	$4.69 \cdot 10^{-7}$
50	$2.44 \cdot 10^{-7}$	$2.40 \cdot 10^{-7}$
85	$1.57 \cdot 10^{-7}$	$1.55 \cdot 10^{-7}$
145	$1.15 \cdot 10^{-7}$	$1.15 \cdot 10^{-7}$

$$\frac{\partial c_l}{\partial t} = u_{avg}\frac{\partial c_l}{\partial x} = -k_{ov,1D}c_l \tag{10}$$

$$k_{ov,1D} \sim k_{m,1D}\frac{A_m}{V} \tag{11}$$

By integrating and considering the initial conditions $t = 0$ and $c = c_0$, the relation between c_{out} and τ provides $k_{ov,1D}$ (s^{-1}). Realise that $k_{ov,1D}$ approaches $k_{m,1D}\frac{A_m}{V}$ if concentration polarisation becomes negligible (A_m is the membrane interfacial area). This occurs when the transverse diffusion is much faster than the membrane permeation. The $k_{m,1D}$ (m s^{-1}) values can therefore be extracted from the experimental data by simple curve fitting using Eq. (10):

$$k_{m,1D} = -\frac{V}{A_m}\cdot\frac{1}{t}\cdot ln\frac{c_{out}}{c_0} \tag{12}$$

Table 1 displays the values of $k_{m,1D}$ and $k_{m,2D}$ for different membrane thicknesses. For the thicker membranes, $k_{m,1D}$ converges to $k_{m,2D}$, which indicates that concentration polarisation becomes negligible.

Realise that our $k_{m,1D}$ consists of the resistances of both the membrane and the boundary layer. k_l can therefore be estimated from Eq. (2) giving values ranging from 10^{-6} to 10^{-5} m s^{-1}. This confirms little concentration polarisation in our system and suggests that our microfluidic PV would benefit from thinner, composite, pervaporation membranes, as opposed to large scale pervaporation processes. For thick membranes, one can determine k_m directly from the 1D equation, where for thin membranes one needs to include the 2D equations that include information on the depletion zone.

A comparison of k_m with k_l reveals that, the acetone separation becomes diffusion limited for very thin (e.g. composite) PDMS membranes. In such cases, k_m approaches k_l around 10^{-6} m s^{-1} and generates a highly efficient pervaporation system. These results demonstrate the advantages of using a microfluidic device in terms of its efficient mass transport caused by relatively short diffusion distances. Further reducing the channel height will benefit the separation process only when k_l is comparable or smaller than k_m.

Fig. 6 displays the concentration profile within the liquid phase as numerically obtained for $k_m = 4.94 \cdot 10^{-7}$ m s^{-1}, corresponding to the 35 μm thick membrane, for two different residence times. As can be seen, a developed concentration profile forms near the channel entrance even at the highest operated flow velocity. This is due to the relatively fast transverse diffusion compare to the convection transport in x direction in our microfluidic channel. By comparing the two timescales for transport in normal ($\perp$ diffusion) and tangential ($\parallel$ convection) direction (Eq. (8)), we obtained a ratio ranging from 0.096 to 0.96. As demonstrated in Fig. 6(b), where Re is 0.084, the normal diffusion results in a nearly constant concentration gradient along the y direction. For such cases, the simplified 1D model accurately describes the performance of the PV process.

To accomplish a quantitative optimisation of the system performance, the separation efficiency can be predicted in terms of the

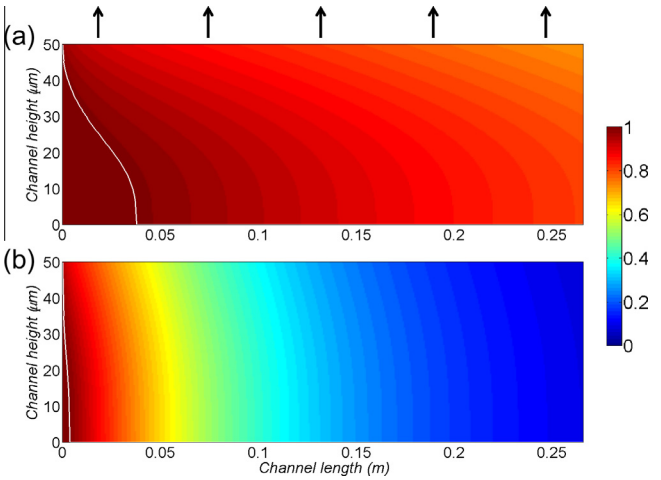

Fig. 6. Local concentration profiles for $k_m = 4.94 \cdot 10^{-7}$ m s^{-1} (35 μm membrane). (a) Residence time = 26 s, Re = 0.84. (b) Residence time = 265 s, Re = 0.084. The white curves indicate the boundary between the bulk ($c_{bulk} >= 99\% c_0$) solution and the depletion zone.

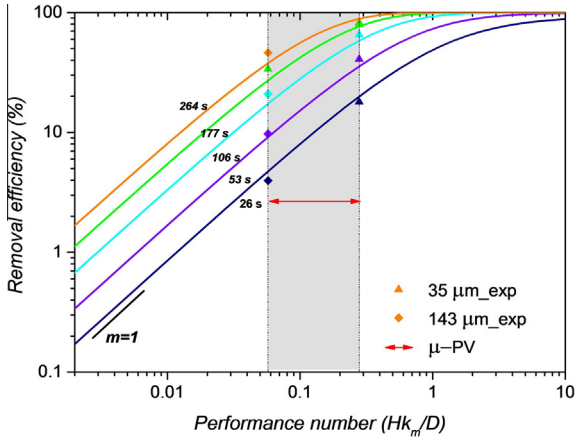

Fig. 7. Dependence of acetone removal efficiency on the performance factor Hk_m/D. Symbols represent the experimental results and lines correspond to the simulations. m represents the symbol for the slope of the curves.

factor Hk_m/D (Fig. 7, for a fixed value of H). This factor sets the boundary flux (as in Eq. (5)) normalised by the diffusive flux. For each residence time, an increase in this ratio, which is an increase in k_m here, enhances the removal efficiency. When membrane transport is limiting, any increase in k_m will result in a proportional increase in removal efficiency, giving a slope equal to 1. As can be seen, the obtained slopes vary from ~1 to <1 with increasing k_m values. The symbols in Fig. 7 indicate the performance of our micro-PV experiments (the grey region), which is at the transition towards the rate limiting regimes. Such findings allow us to identify whether mass transport in the fluid phase or in the membrane is rate limiting and the extend of improvement that can be obtained.

5. Conclusions

Implementing pervaporation into a microfluidic device is presented to study VOC removal from aqueous solutions. An acetone removal efficiency of 81% is achieved within just 3 min at room temperature by a 35 μm thick PDMS membrane. The use of a microfluidic format drastically improves mass transport in the boundary layer, which provides adequate membrane performance

assessment. The derived performance number, Hk_m/D, based on the intrinsic system parameters is capable in assisting process design for both micro-and macro-scales. Our microfluidic device shows promising potential as a universal tool for the removal of various volatile organic components (VOCs) by pervaporation.

Acknowledgements

The authors would like to acknowledge the Dutch Technology Foundation STW (project 11396) for the financial support. We would like to thank Micronit B.V. (Netherlands) for the fabrication of microchips, Dr Jeff Wood and Sander Haase for helpful discussions and Ineke Punt for the experimental assistance.

References

[1] O. Wörz, K. Jäckel, T. Richter, A. Wolf, Microreactors, a new efficient tool for optimum reactor design, Chem. Eng. Sci. 56 (3) (2001) 1029–1033, http://dx.doi.org/10.1016/S0009-2509(00)00318-3.
[2] G.N. Doku, W. Verboom, D.N. Reinhoudt, A. van den Berg, On-microchip multiphase chemistry-a review of microreactor design principles and reagent contacting modes, Tetrahedron 61 (11) (2005) 2733–2742, http://dx.doi.org/10.1016/j.tet.2005.01.028.
[3] V. Hessel, A. Renken, J.C. Schouten, Handbook of Micro-Reactor Engineering and Chemistry, Wiley-VCH, 2006.
[4] N.T. Nguyen, Z. Wu, Micromixers-a review, J. Micromech. Microeng. 15 (2005) R1–R16, http://dx.doi.org/10.1088/0960-1317/15/2/R01.
[5] V. Hessel, H. Löwe, F. Schönfeld, Micromixers-a review on passive and active mixing principles, Chem. Eng. Sci. 60 (8–9) (2005) 2479–2501, http://dx.doi.org/10.1016/j.ces.2004.11.033.
[6] K.F. Lam, E. Sorensen, A. Gavriilidis, Review on gas–liquid separations in microchannel devices, Chem. Eng. Res. Des. 91 (10) (2013) 1941–1953, http://dx.doi.org/10.1016/j.cherd.2013.07.031.
[7] E.Y. Kenig, Y. Su, A. Lautenschleger, P. Chasanis, M. Grünewald, Micro-separation of fluid systems: a state-of-the-art review, Sep. Purif. Technol. 120 (2013) 245–264, http://dx.doi.org/10.1016/j.seppur.2013.09.028.
[8] R.L. Hartman, K.F. Jensen, Microchemical systems for continuous-flow synthesis, Lab Chip 9 (17) (2009) 2495–2507, http://dx.doi.org/10.1039/b906343a.
[9] R.L. Hartman, J.R. Naber, S.L. Buchwald, K.F. Jensen, Multistep microchemical synthesis enabled by microfluidic distillation, Angew. Chem. Int. Ed. Engl. 49 (5) (2010) 899–903, http://dx.doi.org/10.1002/anie.200904634.
[10] B.S. Broyles, S.C. Jacobson, J.M. Ramsey, Sample filtration, concentration, and separation integrated on microfluidic devices, Anal. Chem. 75 (11) (2003) 2761–2767, http://dx.doi.org/10.1021/ac025503x.
[11] D. Webb, T.F. Jamison, Continuous flow multi-step organic synthesis, Chem. Sci. 1 (6) (2010) 675, http://dx.doi.org/10.1039/c0sc00381f.
[12] T. Chan, G. Priestman, J. MacInnes, R. Allen, Development of a micro-channel contactorseparator for immiscible liquids, Chem. Eng. Res. Des. 86 (1) (2008) 65–74, http://dx.doi.org/10.1016/j.cherd.2007.10.010.
[13] F. Scheiff, M. Mendorf, D. Agar, N. Reis, M. Mackley, The separation of immiscible liquid slugs within plastic microchannels using a metallic hydrophilic sidestream, Lab Chip 11 (2011) 1022–1029, http://dx.doi.org/10.1039/C0LC00442A.
[14] Y. Zhang, S. Kato, T. Anazawa, Vacuum membrane distillation by microchip with temperature gradient, Lab Chip 10 (7) (2010) 899–908, http://dx.doi.org/10.1039/b915534a.
[15] Y. Kaufman, R. Kasher, V. Freger, Microfluidic NF/RO separation: cell design, performance and application, J. Membr. Sci. 396 (2012) 67–73, http://dx.doi.org/10.1016/j.memsci.2011.12.052.
[16] B. Smitha, D. Suhanya, S. Sridhar, M. Ramakrishna, Separation of organic-organic mixtures by pervaporation-a review, J. Membr. Sci. 241 (1) (2004) 1–21, http://dx.doi.org/10.1016/j.memsci.2004.03.042.
[17] X. Feng, R.Y. Huang, Liquid separation by membrane pervaporation : a review, Ing. Eng. Chem. Res. 36 (4) (1997) 1048–1066, http://dx.doi.org/10.1021/ie960189g.
[18] J.-S. Jiang, L.M. Vane, S.K. Sikdar, Recovery of VOCs from surfactant solutions by pervaporation, J. Membr. Sci. 136 (1997) 233–247, http://dx.doi.org/10.1016/S0376-7388(97)00169-5.
[19] T. Zeng, A.J. McCabe, T.C. Frank, J.K. Carpenter, W.A. Arnold, E.L. Cussler, Membrane-assisted volatile organic compound removal from aqueous acrylic latex is faster than from aqueous solutions, Ind. Eng. Chem. Res 53 (31) (2014) 12420–12427, http://dx.doi.org/10.1021/ie5012239.
[20] B. Ulrich, T.C. Frank, A. McCormick, E. Cussler, Membrane-assisted voc removal from aqueous acrylic latex, J. Membr. Sci. 452 (2014) 426–432, http://dx.doi.org/10.1039/b822106e.
[21] S. Ramprasad, J.D. Palmer, A silicon microseparator based pervaporation process for separation of ethanol/water mixtures using a polymer membrane, Sep. Sci. Technol. 42 (11) (2007) 2483–2499, http://dx.doi.org/10.1080/01496390701477170.
[22] J. Leng, B. Lonetti, P. Tabeling, Micro-evaporators for kinetic exploration of phase diagrams, Phys. Rev. Lett. 96 (8) (2006) 084503, http://dx.doi.org/10.1103/PhysRevLett. 96.084503.
[23] S. Camou, A. Shimizu, T. Horiuchi, T. Haga, Selective aqueous benzene detection at ppb level with portable sensor based on pervaporation extraction and UV-spectroscopy, Proc. Chem. 1 (1) (2009) 1495–1498, http://dx.doi.org/10.1016/j.proche.2009.07.373.
[24] I. Ziemecka, B. Haut, B. Scheid, Hydrogen peroxide concentration by pervaporation of a ternary liquid solution in microfluidics, Lab Chip 15 (2015) 504–511, http://dx.doi.org/10.1039/C4LC00886C.
[25] L. Daubersies, J. Leng, J.-B. Salmon, Steady and out-of-equilibrium phase diagram of a complex fluid at the nanolitre scale: combining microevaporation, confocal Raman imaging and small angle X-ray scattering, Lab Chip 13 (5) (2013) 910–919, http://dx.doi.org/10.1039/c2lc41207a.
[26] M. Schindler, A. Ajdari, Modeling phase behavior for quantifying micro-pervaporation experiments, Eur. Phys. J. E Soft Matter 28 (1) (2009) 27–45, http://dx.doi.org/10.1140/epje/i2008-10419-y.
[27] F. Lipnizki, G. Trägårdh, Modelling of pervaporation: models to analyze and predict the mass transport in pervaporation, Sep. Purif. Methods 30 (1) (2001) 49–125, http://dx.doi.org/10.1081/SPM-100102985.
[28] H.O. Karlsson, G. Trägårdh, Pervaporation of dilute organic-waters mixtures. A literature review on modelling studies and applications to aroma compound recovery, J. Membr. Sci. 76 (1993) 121–146, http://dx.doi.org/10.1021/ie960189g.
[29] A. Noworyta, M. Kubasiewicz-Ponitka, A. Koziol, Mass and heat transport resistance in pervaporation process, Desalin. Water Treat. 26 (1–3) (2011) 226–235, http://dx.doi.org/10.5004/dwt.2011.1502.
[30] E.L. Cussler, Diffusion: Mass Transfer in Fluid Systems, Cambridge University Press, 2009.
[31] P. Côté, C. Lipski, Reducing concentration polarization in pervaporation for trace contaminant removal, in: Proc. 1990 Int. Cong. Memb. Memb. Proc., Chicago, 1990, p. 325.
[32] C. Lipski, P.L. Côté, The use of pervaporation for the removal of organic contaminants from water, Environ. Prog. 9 (4) (1990) 254–261, http://dx.doi.org/10.1002/ep.670090420.
[33] T.M. Squires, R.J. Messinger, S.R. Manalis, Making it stick: convection, reaction and diffusion in surface-based biosensors, Nat. Biotechnol. 26 (4) (2008) 417–426, http://dx.doi.org/10.1038/nbt1388.
[34] J.G. Wijmans, A.L. Athayde, R. Daniels, J.H. Ly, H.D. Kamaruddin, I. Pinnau, The role of boundary layers in the removal of volatile organic compounds from water by pervaporation, J. Membr. Sci. 109 (1) (1996) 135–146, http://dx.doi.org/10.1016/0376-7388(95)00194-8.
[35] L. Li, Z. Xiao, S. Tan, L. Pu, Z. Zhang, Composite PDMS membrane with high flux for the separation of organics from water by pervaporation, J. Membr. Sci. 243 (1–2) (2004) 177–187, http://dx.doi.org/10.1016/j.memsci.2004.06.015.
[36] I. Blume, J.G. Wijmans, R.W. Baker, The separation of dissolved organics from water by pervaporation, J. Membr. Sci. 49 (1990) 253–286, http://dx.doi.org/10.1016/S0376-7388(00)80643-2.
[37] M. Hollein, M. Hammond, C. Slater, Concentration of dilute acetone-water solutions using pervaporation, Sep. Sci. Technol. 28 (4) (1993) 1043–1061, http://dx.doi.org/10.1080/01496399308029237.
[38] H.H. Nijhuis, Removal of trace organics from water by pervaporation: a technical and economic analysis (Ph.D. thesis), University of Twente, 1990.
[39] K. Aran, L.A. Sasso, N. Kamdar, J.D. Zahn, Irreversible, direct bonding of nanoporous polymer membranes to pdms or glass microdevices, Lab Chip 10 (5) (2010) 548–552, http://dx.doi.org/10.1039/b924816a.
[40] S.X. Liu, M. Peng, Verification of mass transfer simulation with CFD using highly accurate solutions, Comput. Electron. Agric. 49 (2) (2005) 309–314, http://dx.doi.org/10.1016/j.compag.2005.05.003.
[41] J.P. Lopes, S.S. Cardoso, A.E. Rodrigues, Criteria for kinetic and mass transfer control in a microchannel reactor with an isothermal first-order wall reaction, Chem. Eng. J. 176 (2011) 3–13, http://dx.doi.org/10.1016/j.cej.2011.05.088.
[42] A. Urtiaga, E. Gorri, J. Beasley, I. Ortiz, Mass transfer analysis of the pervaporative separation of chloroform from aqueous solutions in hollow fiber devices, J. Membr. Sci. 156 (1999) 275–291, http://dx.doi.org/10.1016/S0376-7388(98)00350-0.